URSI AP-RASC, Sydney, Australia, 17 – 22 August 2025

Comparison between Beam-Forming and Orthogonality Sampling Method

A. Cuccaro*(1), A. Dell'Aversano(2), M.A. Maisto(2), G. Leone(2), and R. Solimene(2)
(1) DIMES, University of Calabria, Rende, Italy
(2) Dept. of Engineering, University of Campania, Aversa, Italy

Abstract

A comparative analysis between the orthogonally sampling method and the beam-forming schemes is presented. In particular, two different versions of the beam-forming are considered: the windowed (i.e. classical approach) and the non-windowed (i.e. non-coherent approach) schemes. By considering, a multiview/multistatic/multifrequency configuration in a 2D geometry, the point spread functions of the different methods are derived. This makes the comparison easier in terms of the achievable resolution and how the configuration parameters affect the performances of the imaging methods. Moreover, the role of the noise and the uncertain antenna frequency response are analyzed. Numerical results confirmed that the non-coherent beam-forming method exhibits the best trade-off between achievable performance and robustness against the noise and antenna uncertainties.

1 Introduction

Microwave imaging are widely used in applications where non-invasive diagnostics or in countless scenarios is required [1, 2]. However, the pertinent inverse scattering problem is hard to solve because of its non-linearity and ill-posedness [3]. Even though significant progress has been made on this framework by exploiting the recent approach based on machine learning [5], the "quantitative" reconstructions stay a challenging task. Differently, the radar imaging provides a "qualitative" information about the scattering scene. In these cases, the problem is drastically simplified. In general, strategies that offers qualitative reconstructions can be categorized as linear inversion methods and indicator based methods.

Linear inversion methods foresee some kind of linearization of the scattering equations [6]. Under this assumption, only information about the positions and the supports of the targets can be retrieved [7]. In principle, all the linear inversion methods [8, 9] are basically wavefront reconstruction techniques that achieve the reconstuction by back-propagating the collected scattered field [10]. A second class of linear reconstruction methods, hence qualitative, are those that aim at building an indicator function that highlights, the supports of the targets inside the image domain [11, 12, 13, 14]. The orthogonality sampling method OSM [15] falls into this category. It has been recently proposed as a fast alternative to other indicator based methods. Both classes of methods are considered as competing methods. Accordingly, in this paper a comparison between linear inversion and indicator methods is presented. Among the linear inversion method, we select the most popular beam-forming (BF) [16] to compare to the OSM. The study is developed for a near-field 2D and scalar scattering configuration, under a multiview/multistatic/multifrequency configuration. In order to achieve the point spread functions (PSF) allowing an immediate and direct comparison between the inversion methods, we consider targets that are small compared to the employed wavelength [17] and we choose to work under the linear Born model [18]. The role of the noise level and antenna uncertainties are analyzed.

2 Scattering Scenario

The scattering scenario is depicted in Figure 1. Here, the scattering problem at hand is two-dimensional and scalar. Indeed, the scenario is invariant along z axis, and the incident field is TM and assumed to be radiated by a filamentary electric current directed along the z-axis.

A multi-static/multi-view measurement configuration is considered. Accordingly, for each transmitting antenna (TX) position, $\underline{r}_i$, the scattered field is collected over different measurement points (RX), $\underline{r}_o$. Both the transmitting and the receiving elements are placed over a circle of radius R which surrounds the scenario of interest. This allows to define the (TX, RX) positions only in terms of the angles $(\theta_i, \theta_o) \in [0, 2\pi) \times [0, 2\pi)$. By reasoning in the freqeuncy domain, the scattered field can be expressed by the following scattering integral equation:

$$U_S(\omega, \theta_i, \theta_o) = (\omega/4v)^2 S(\omega) \times \int_D H_0^{(2)}\left[\frac{\omega}{v}|\underline{r} - \underline{r}_i|\right] H_0^{(2)}\left[\frac{\omega}{v}|\underline{r}_o - \underline{r}|\right] \chi(\underline{r}) d\underline{r} \qquad (1)$$

where the Born approximation is employed [18]. Moreover, $1/4jH_0^{(2)}(\cdot)$ is the two-dimensional scalar Green function, $H_0^{(2)}(\cdot)$ is the Hankel function of second type and zero order, $U_S(\omega, \theta_i, \theta_o)$ is the scattered field data, v the background propagation speed and D the spatial region

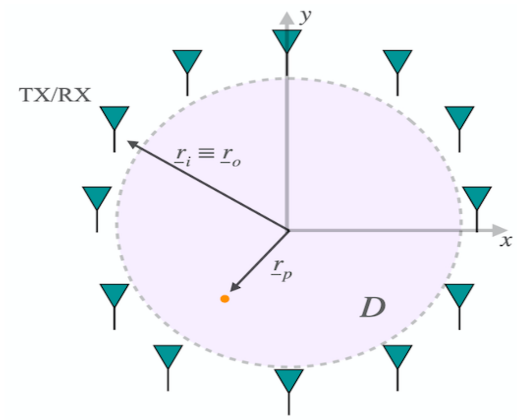

Figure 1. Pictorial view of the scattering scene. Invariance is assumed along the z-axis.

under investigation. Note that for simplicity, the background medium is assumed homogeneous, non-magnetic and lossless. $\chi(\underline{r}) = \varepsilon(\underline{r})/\varepsilon_b - 1$ is the object function, with $\varepsilon(\underline{r})$ and ε_b being the dielectric permittivity of the object and of the background, respectively. Finally, the term enclosed the antenna resonse. Indeed, $S(\omega) = j\omega\mu_0 H_{RX}(\omega)H_{TX}(\omega)P(\omega)$, where $P(\omega)$ is the Fourier spectrum of the transmitted pulse, $H_{RX}(\omega)$ and $H_{TX}(\omega)$ are the receiving and transmitting antennas' frequency responses and the term $j\omega\mu_0$, μ_0 being the magnetic permeability of the vacuum, is due to the incident field. Finally, $\exp(j\omega t)$, represents the time convention with ω being the angular frequency,

3 Image Methods

In this section we introduce the basic elements of the BF and OSM methods whereas all the mathematical details can be found in [19].The classical BF based on two step: first a time-shifting to isolate signals reflected from a particular synthetic point within the areas under investigation, and then summing the signals. The synthetic point is then scanned to create the image. This suggest that the natural implementation of BF is in time domain, where a properly time window $W(t)$ need to adopted. In [19], two limit cases are considered: the non-windowed case (i.e $W(t)$ is absent) and when $W(t) = \delta(t)$.

3.0.1 Non Windowed BF

When the BF is implemented in the frequency domain and the $W(t)$ is absent, the reconstruction can be written as:

$$I_{BFNW}(\underline{r}) = \int_\Omega \left| \int_0^{2\pi}\int_0^{2\pi} U_S(\omega,\theta_i,\theta_o)\exp[j\omega\tau(\theta_i,\theta_o,\underline{r})]d\theta_i d\theta_o \right|^2 d\omega \quad (2)$$

where Ω is the bandwidth of the transmitted pulse and the subscript $BFNW$ stands for beam-forming for the non-windowed case. In order to estimate the resolution, we need to evaluate the properties of the point-spread function

$$PSF_{BFNW}(\underline{r},\underline{r}_p) = \frac{v\pi^2}{4R^4}\int_{\Omega_k} k^2 J_0^4(k|\underline{r}-\underline{r}_p|)dk \quad (3)$$

where $k = \omega/v$ is the wavenumber and Ω_k is the corresponding bandwidth.

3.0.2 Windowed BF

Now we focus on the role of the time window $W(t)$. In particular, for $W(t) = \delta(t)$ the beam-forming reconstruction becomes:

$$I_{BFW}(\underline{r}) = \left| \int_\Omega \int_0^{2\pi}\int_0^{2\pi} U_S(\omega,\theta_i,\theta_o)\exp[j\omega\tau(\theta_i,\theta_o,\underline{r})]d\theta_i d\theta_o d\omega \right|^2 \quad (4)$$

here, of course, BFW is a reminder that we are under the windowed case. Equations (2) and (4) are interesting since they establish that the no -windowed and windowed case in time domain, in frequency domain results in non-coherent and coherent summation, respectively. In this case the point-spread function PSF_{BFW} is:

$$PSF_{BFW}(\underline{r},\underline{r}_p) = \frac{v^2\pi^2}{4R^4}\left(\int_{\Omega_k} kJ_0^2(k|\underline{r}-\underline{r}_p|)dk\right)^2 \quad (5)$$

3.0.3 Ortogonality Sampling Method

In near field, the orthogonality sampling method builds the following indicator to highlight the scatterers' supports

$$I_{OSM}(\underline{r}) = \int_\Omega \int_0^{2\pi} \frac{2v}{\omega\pi}\left| \int_0^{2\pi} \frac{U_S(\omega,\theta_i,\theta_o)}{\sqrt{|\underline{r}-\underline{r}_o|}}\exp[j\omega\tau_o(\theta_o,\underline{r})]d\theta_o \right|^2 d\theta_i d\omega \quad (6)$$

Comparing (2),(4) and (6) it is clear that the back-propagation step is embodied within the two different methods. The difference is the way both approaches attempt to refocus the scattered field. For the PSF, the following equation hold:

$$PSF_{OSM}(\underline{r},\underline{r}_p) = \frac{v}{4R^3}\int_{\Omega_k} kJ_0^2(k|\underline{r}-\underline{r}_p|)dk \quad (7)$$

.

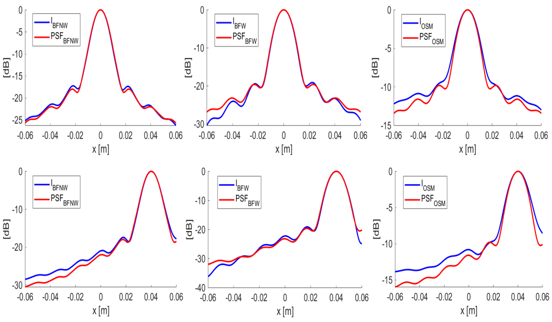

Figure 2. Comparing normalized point-spread functions returned by eqs. (2), (4), and (6) (denoted as I_{BFNW}, I_{BFW}, and I_{OSM}) against (3), (5) and (7) (denoted as PSF_{BFNW}, PSF_{BFW}, and PSF_{OSM}). Cut views along the x axis are displayed for two scatterer's locations, $(0,0)$ (top panels) and $(0.4\lambda_m, 0)$ (bottom panels), where λ_m is the wavelength corresponding to the minimum employed frequency. Background medium velocity is $v = c/3$ and the frequency band is $[1,3]$ GHz.

4 Numerical Results

Initially, the goodness of the PSF estimated given by (3), (5) and (7) are compared with respective reconstructions (2), (4) and (6) when a point-like scatterer is considered. Figure 2 summarizes the results. In particular, in the panels on the left column refers to non windowed beam-forming, highlighting that the two PSFs practically overlap. As can be seen, very minor deviations occur only outside the main beam. Similar considerations apply to panels in the middle column, where the windowed beam-forming are depicted. Finally, panels in the right column of the same Figure shows the excellent agreement between the analytical and the actual PSF for OSM method. Finally, in Figure 3 the effect of uncertain phase antenna response and noise are both considered. As can seen, the windowed case shows a significant loss in the focusing ability.

5 Conclusions

In this work, the classical inverse scattering problem of imaging small targets have been considered. Two beam-forming schemes have been compared, i.e, the BF_{NW}, BF_{W} and the OSM, for a multistatic-multiview near-field configuration and a two-dimensional scalar geometry.

Numerical results confirmed the goodness of the PSFs which allow to estimate the achievable resolution. Moreover, numerical results suggest that the non-windowed BF and the OSM are better suited for realistic near-field applications, but the non-windowed BF is preferable because it is more stable against the noise.

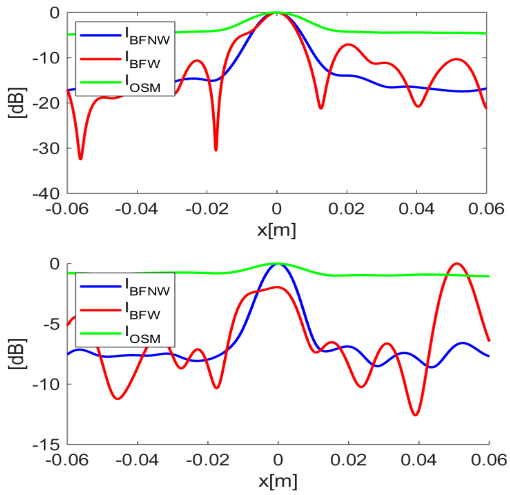

Figure 3. Cut view along the x-axis of the normalized reconstruction of a scattering point object located at $(0,0)$ for two realizations of $\phi(\omega)$ with SNR -10 dB (top panel) and SNR -20 dB (bottom panel).

References

[1] M. Pastorino and A. Randazzo, *Microwave imaging methods and applications.* Boston, MA, USA: Artech House, 2018.

[2] X. Chen, *Computational methods for electromagnetic inverse scattering*. Singapore: John Wiley and Sons, 2018.

[3] I. Catapano, A. Randazzo, E. Slob, R. Solimene, *GPR imaging via qualitative and quantitative approaches.* In Civil Engineering Applications of Ground Penetrating Radar, Benedetto, A. and Pajewski, L. (eds). Springer International Publishing, Cham, 2015.

[4] L. Di Donato, M. T. Bevacqua, L. Crocco, T. Isernia, "Inverse scattering via virtual experiments and contrast source regularization," *IEEE Transactions on Antennas and Propagation*, **63**, no. 4, 2015, pp. 1669–1677, doi: 10.1109/TAP.2015.2392124.

[5] L. Li, L. G. Wang, F. L. Teixeira, C. Liu, A. Nehorai, T. J. Cui, "DeepNIS: Deep neural network for nonlinear electromagnetic inverse scattering," *IEEE Transactions on Antennas and Propagation*, **67**, no. 8, 2019, pp. 1819–1825, doi: 10.1109/TAP.2018.2885437.

[6] D. L. Marks, "A family of approximations spanning the Born and Rytov," *Optics Express*, **14**, no. 19, 2006, pp. 8837–8848, doi: 10.1364/OE.14.008837.

[7] G. Gennarelli, I. Catapano, F. Soldovieri, R. Persico, "On the achievable imaging performance in full 3-D linear inverse scattering," *IEEE Transactions on Antennas and Propagation*, **63**, no. 3, 2015, pp. 1150–1155, doi: 10.1109/TAP.2014.2387421.

[8] S. C., Hagness, A. Taove, and J. E. Bridges, “Two-dimensional FDTD analysis of a pulsed microwave confocal system for breast cancer detection: fixed focus and antenna array sensors," *IEEE Transaction on Biomedical Engineering*, **45**, no. 12, 1998, pp. 1470-1479, doi: 10.1109/10.730440.

[9] R. H. Stolt, “Migration by Fourier transform," *Geophysics*, **43**, 1978, pp. 23-48, doi: 10.1190/1.1440826.

[10] R. Solimene, I. Catapano, G. Gennarelli, A. Cuccaro, A. Dell'Aversano and F. Soldovieri, “SAR imaging algorithms and some unconventional applications: a unified mathematical overview," *IEEE Signal Processing Magazine*, **31**, no. 4, 2014, pp. 90-98, doi: 10.1109/MSP.2014.2311271.

[11] F. Cakoni, D. Colton, *Qualitative methods in inverse scattering theory*. Berlin: Springer, 2006.

[12] A. Kirsch, N. Grinberg, *The factorization method for inverse problems*. Oxford: Oxford University Press, 2008.

[13] D. R. Luke, R. Potthast, “The no response test - a sampling method for inverse scattering problems," *SIAM Journal of Applied Mathematics*, **63**, no.4, 2003, pp. 1292–312, doi: 10.1137/S0036139902406887

[14] R. Potthast, “A survey about sampling and probe methods for inverse problems," *Inverse Problems*, **22**, 2006, doi: 10.1088/0266-5611/22/2/R01.

[15] R. Potthast, “A study on orthogonality sampling," *Inverse Problems*, **26**, 2010, doi: 10.1088/0266-5611/26/7/074015.

[16] R. Solimene, A. Cuccaro, G. Ruvio, D. F. Tapia, M. O'Halloran, “Beamforming and holography image formation methods: An analytic study,"*Optics Express*, **24**, no. 8, 2016, pp. 9077-9093, doi: 10.1364/OE.24.009077.

[17] R. Solimene, A. Brancaccio, J. Romano, R. Pierri, “Localizing thin metallic cylinders by a 2.5-D linear distributional approach: experimental results," *IEEE Transactions on Antennas and Propagation*, **56**, no. 8, 2008, pp. 2630-2637, doi: 10.1109/TAP.2008.927506

[18] W. C. Chew, *Waves and fields in inhomogeneous media*. New York: Van Nostrand Reinhold, 1990.

[19] A. Cuccaro, A. Dell'Aversano, M. A. Maisto, G. Leone and R. Solimene, "Microwave Imaging of Small Scatterers: Linking and Comparing the Beam-Forming and the Orthogonality Sampling Method," *IEEE Transactions on Antennas and Propagation*, 2025, doi: 10.1109/TAP.2025.3531661.